Optically pumped deep-UV multimode lasing in AlGaN double heterostructure grown by molecular beam homoepitaxy

Cite as: AIP Advances 12, 035023 (2022); doi: 10.1063/5.0085365
Submitted: 15 January 2022 • Accepted: 23 February 2022 •
Published Online: 11 March 2022

Len van Deurzen,[1,a] Ryan Page,[2] Vladimir Protasenko,[3] Kazuki Nomoto,[3] Huili (Grace) Xing,[2,3] and Debdeep Jena[1,2,3]

AFFILIATIONS

[1] Department of Applied and Engineering Physics, Cornell University, Ithaca, New York 14853, USA
[2] Department of Materials Science and Engineering, Cornell University, Ithaca, New York 14853, USA
[3] Department of Electrical and Computer Engineering, Cornell University, Ithaca, New York 14853, USA

[a] Author to whom correspondence should be addressed: lhv9@cornell.edu

ABSTRACT

Multimode lasing at sub-300 nm wavelengths is demonstrated by optical pumping in AlGaN heterostructures grown on single-crystal AlN substrates by plasma-assisted molecular beam epitaxy. Edge-emitting ridge-based Fabry–Pérot cavities are fabricated with the epitaxial AlN/AlGaN double heterostructure by a combined inductively coupled plasma reactive ion etch and tetramethylammonium hydroxide etch. The emitters exhibit peak gain at 284 nm and modal linewidths on the order of 0.1 nm at room temperature. The applied growth technique and its chemical and heterostructural design characteristics offer certain unique capabilities toward further development of electrically injected AlGaN laser diodes.

High output power semiconductor UV-B (280–315 nm) and UV-C (100–280 nm) emitters are desirable as they are energy-efficient and compact photonic devices with diverse applications. These include pathogen detection and sterilization,[1,2] water purification,[3] gas sensing,[4] photolithography,[5] and quantum computing and metrology,[6,7] to name a few. The realization of continuous-wave electrically injected UV-C laser diodes (LDs) based on the AlGaN semiconductor material system remains challenging, as these wide-bandgap semiconductors exhibit low carrier mobilities, very large dopant activation energies, resulting in low free carrier concentrations, and asymmetries between electron and hole transport.[8,9] This makes it a challenge to achieve population inversion and sufficient gain by electrical injection. Nonetheless, electrically pumped lasers with low optical loss in the UV-B and UV-C range have recently been demonstrated by metal organic chemical vapor deposition (MOCVD),[10,11] and progress has been made to reduce the current densities and voltages required for lasing.[12,13] However, with these advancements, all demonstrated laser diodes emitting below 348 nm currently operate under pulsed mode, limiting their practicality.[14]

In optically pumped AlGaN lasers, on the other hand, population inversion is predominantly achieved by local generation of electron–hole pairs instead of by drift and diffusion currents and therefore do not suffer from severe gain challenges. Consequently, optically pumped lasing has been achieved in AlGaN heterostructures grown by MOCVD on bulk AlN[15] and AlN/sapphire templates.[16] Much less study has been done on stimulated emission in AlGaN thin films grown by molecular beam epitaxy (MBE), with reports of stimulated emission only reported on AlGaN thin films grown on sapphire[17–19] and SiC.[20] These studies have shown the influence of implementing multiple quantum wells and graded polarization layers as a waveguide, and the effect of such design parameters as well as growth conditions on the amplified spontaneous emission (ASE) threshold. However, these reports by MBE exhibit wide photoluminescence linewidths on the order of a few nm and have not shown any evidence of longitudinal mode formation,

which is a signature of lasing in Fabry–Pérot resonators. Moreover, heteroepitaxy on foreign substrates results in a large threading dislocation density of $\gtrsim 10^8/cm^2$, leading to optical intrinsic loss and reduced optical gain due to the scattering of the optical cavity modes and free carriers.[21,22]

With the development of molecular beam homoepitaxy, where AlGaN films are grown on bulk AlN substrates, the optical intrinsic loss can be kept low by reducing the threading dislocation density ≈ millionfold. This also results in a reduction in the point defect density compared to growth on foreign substrates, such as SiC, sapphire, and templates.[23,24] MBE also offers certain advantages over MOCVD. For instance, MBE-grown thin films show a low O, H, and C impurity background, and atomically sharp heterostructure interfaces can be grown. This is useful for the growth of tunnel junctions, short-period superlattices (SPSLs), or monolayer thick multiple quantum wells.[25] Besides, there are no memory- or chemical activation-effects present for Mg doping, allowing for the growth of buried, conductive *p*-type layers. This enables inverted diode structures, where spontaneous polarization fields stemming from sheet charging at heterostructure interfaces are favorably aligned with the applied field to enhance carrier injection and reduce carrier overflow. This has recently been achieved in tunnel junction based (*n-p-i-n*) AlN/GaN/InGaN light-emitting diodes.[26,27]

In this work, we report the observation of laser oscillation in an optically pumped sub-300 nm AlGaN double heterostructure grown by molecular beam epitaxy on single crystal AlN by processing them into ridge-based edge-emitters. The double heterostructure Fabry–Pérot laser bars exhibit multi-mode emission with peak gain at $\lambda_0 \approx 284$ nm and low modal linewidths of order $\Delta\lambda \approx 0.1$ nm, an order of magnitude lower than any other reports of UV-lasing by MBE thus far.

The double heterostructure lasers reported here are grown by plasma assisted MBE (PA-MBE) on Al-polar, c-plane single crystal AlN substrates with a dislocation density on the order of 10^4 cm^{-2}. The epistructural layer schematic is shown in Fig. 1(a). Prior to introduction to the MBE chamber, the substrates are cleaned with acids to partially remove surface oxides and contaminants, following a procedure reported previously.[23] Immediately before growth, the substrates undergo a second cleaning process consisting of repeated cycles of aluminum deposition and thermal desorption to further remove native oxide layers and enable dislocation-free nucleation. For all samples, a high substrate temperature (T_{sub} ≈ 1000 °C) AlN buffer layer is grown with a thickness of 1 μm to isolate the active region of the device from the remaining impurities present at the substrate interface, which can contribute to optical loss. Following the buffer layer growth, all excess Al is thermally desorbed and the substrate temperature is lowered to ≈800 °C for the growth of the subsequent AlGaN layers. A bottom waveguide is then grown, targeted at a thickness of 150 nm to confine the optical field and remove the principal lasing mode peak from the AlN–$Al_{0.8}Ga_{0.2}N$ interface, to limit the optical loss from surface-riding impurities formed around that interface.[28] Then, a 20 nm thick quantum well gain layer is grown aimed at an aluminum composition of 55%, followed by a 10 nm $Al_{0.8}Ga_{0.2}N$ cap layer. Excess metal is thermally desorbed from the crystal surface at each heterointerface to ensure sharp interfaces and abrupt compositional change.

A wide 20 nm single quantum well (SQW) active region is chosen as the gain medium, which has been calculated to produce substantial gain between excited electron and hole energy levels, where the lower energy level electrons and holes act as screening carriers for the polarization charge that is formed at the heterojunction interfaces.[29] The cap layer thickness is then designed to maximize the product of the optical confinement factor, Γ, and the optical gain, *g*. For the quantum well composition of $Al_{0.55}Ga_{0.45}N$, the lasing cavity modes are transverse electric (TE) polarized. For the asymmetric waveguide design employed here, Γ increases for increasing cap layer thickness.[30] On the other hand, due to generation and recombination of electron–hole pairs in the $Al_{0.8}Ga_{0.2}N$ cap layer upon optical pumping from the surface, the gain of the double heterostructure laser exponentially decreases as a function the cap layer thickness for a given pump intensity. These competing effects are simulated using an optical AlGaN heterostructure solver, STR SiLENSe.[31] The resulting product Γ*g* is found to be maximized at a cap layer thickness of 10 nm when pumping the double heterostructure from the topside with a 193 nm ArF excimer laser. Such an ArF laser is

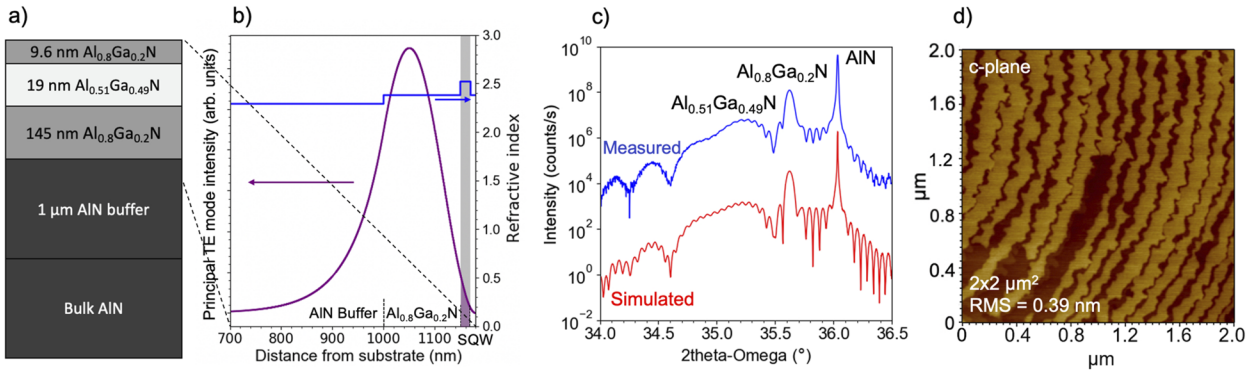

FIG. 1. (a) Schematic of the double heterostructure AlGaN laser with (b) the simulated principal TE optical mode and refractive index. (c) Measured (blue) and simulated (red) 2θ-ω x-ray diffraction scans of the quantum heterostructure in (a) around the [0002] wurtzite symmetry axis. (d) Atomic force microscopy image of the c-plane surface with distinct atomic steps.

employed as the source of population inversion for the AlGaN double heterostructure laser reported here. A schematic of the double heterostructure laser, the accompanying principal TE polarized optical mode, and the 2θ-ω x-ray diffraction (XRD) scan and simulation around the [0002] wurtzite axis are shown in Figs. 1(a)–1(c). The simulated XRD plot in Fig. 1(c) is obtained using the software PANalytical X'Pert Epitaxy with the assumption that the epitaxial AlGaN layers are strained to AlN, which was confirmed with a reciprocal space map (not shown). The measured thicknesses and composition are close to the target and are given in Fig. 1(a). Figure 1(d) shows an atomic force microscopy image of the c-plane surface of the grown double heterostructure laser. Atomic steps due to the miscut angle of the substrate surface are visible. Along with the low rms roughness of 0.39 nm, they indicate that the heterostructure was grown in the desired two-dimensional growth mode.

The epistructure in Fig. 1(a) was fabricated into ridge based etched and cleaved facet emitters. To achieve sufficient optical feedback, imperfections such as slanted and roughened facets that cause a phase shift of the specularly reflected cavity modes, resulting in optical loss, should be avoided. For laser diodes oscillating at shorter wavelengths, the optical loss due to facet imperfections increases superlinearly with the inverse wavelength,[32,33] highlighting the importance of processing optimization for deep-UV laser diodes. This is especially important for electrically injected AlGaN based laser diodes, where it is more difficult to obtain optical gain due to the inherent electronic material properties of wide-bandgap AlGaN.[8]

To achieve vertical facets and sidewalls for the etched emitters, a chlorine-based inductively coupled reactive-ion etching (ICP-RIE) followed by a tetramethylammonium hydroxide (TMAH) wet etch at room temperature for 10 minutes is applied. A similar etching technique was shown to form vertical walls from planar AlGaN heterostructures by Yasue *et al.*[34] In Fig. 2(a), a 70° tilted angle SEM image corresponding to an ICP-RIE dry etch of bulk AlN using a circular Cr/Ni mask is shown, which corresponds to etched sidewalls that are slanted at an angle of ~30° with the *c*-axis, resulting in practically zero reflectance.[32] Therefore, the TMAH wet etch is applied to produce vertical etched facets and enable feedback from the laser cavity. Figure 2(b) shows an SEM image corresponding to the same region as Fig. 2(a) following ICP-RIE and 10 min of TMAH at room temperature. The slanted sidewalls due to ICP-RIE have been formed in to vertical sidewalls by the TMAH wet etch, which is isotropic in the wurtzite m- and *a*-axes with the Cr/Ni mask. After wet etching, at the bottom of the as etched surface, a shallow foothill is formed, and the etch is performed deep enough to remove the optical mode from such a foothill. A ridge based laser design is chosen, as the sidewalls of such a structure improve the intensity and thus photon density and optical gain in the active region compared to planar edge emitters due to lateral optical and carrier confinement. Figure 2(c) shows an SEM image of etched facet emitters, where the as described etching process was applied to form the ridge and mirror facets from the heterostructure shown in Fig. 1(a).

On the other hand, vertical and smooth facets can also be obtained by cleaving. Such cleaved facet emitters were formed by cleaving along the wurtzite m-plane after ICP-RIE, followed by a similar TMAH wet etch, and an SEM image of a device is shown in Fig. 2(d). The surface roughness of the cleaved bulk AlN underneath the laser facet after TMAH treatment was measured using atomic force microscopy, as shown in Fig. 2(e). A low rms roughness of

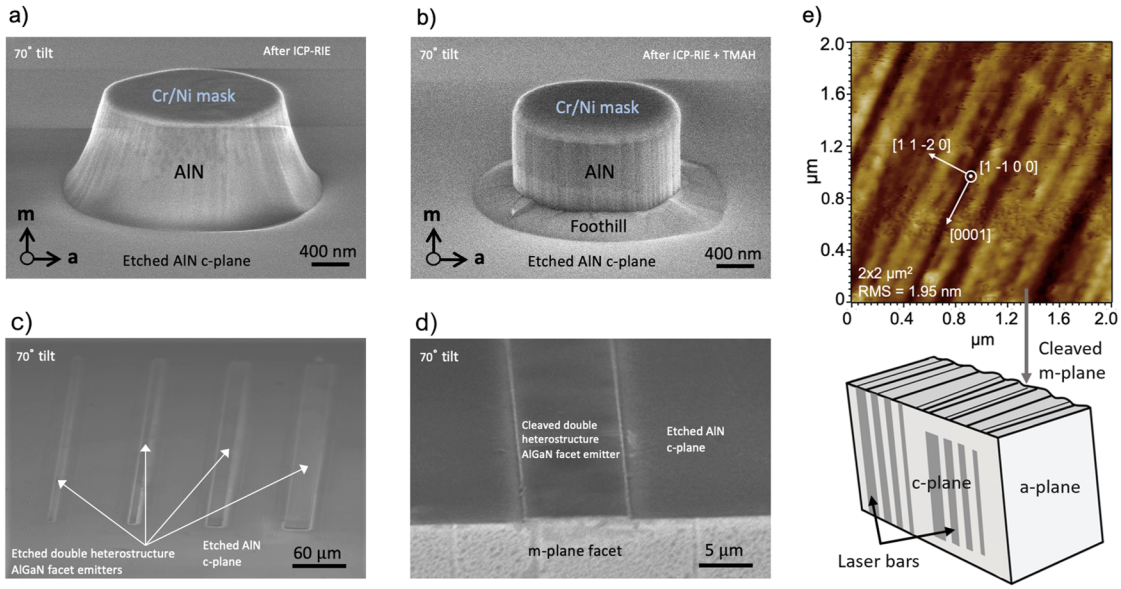

FIG. 2. (a) SEM image of etched AlN by ICP-RIE using a Cr/Ni circular mask enabling the formation of slanted walls. (b) SEM image of etched AlN by ICP-RIE, followed by 10 min TMAH etch at room-temperature enabling the formation of isotropic, vertical walls with a shallow foothill. (c) SEM image of etched facet emitters formed from the heterostructure in Fig. 1(a). (d) SEM image of a cleaved facet emitter formed from the heterostructure in Fig. 1(a). (e) 2 × 2 μm^2 atomic force microscopy image of a facet after cleaving and TMAH etching, with an illustration depicting the imaged m-plane.

1.95 nm was obtained, predominantly due to striations along the *a*-axis, corresponding to a theoretical mirror loss of ≈1.4 cm^{-1} for a ridge length of 1 mm, using a Gaussian roughness approximation as described by Stocker *et al.* in Ref. 33.

An ArF excimer laser emitting at 193 nm (6.42 eV) is used as the optical pump for the AlGaN laser bars and is pulsed at a width of 10 ns at 2 mJ per pulse with a repetition frequency of 100 Hz. The excitation pattern is focused into a pencil shape by cylindrical lenses for uniform excitation of the top of the double heterostructure laser, and the intensity is varied through the use of deep-ultraviolet optical filters. The emission is collected from the Fabry–Pérot facet, and its spectrum is measured with a 500 mm focal length spectrometer with diffraction grating of 2400 lines/millimeter with 240 nm blaze wavelength. All measurements are performed at room temperature. The device and excitation setup is illustrated in the schematic in Fig. 3(a).

Figure 3(b) shows the low resolution photoluminescence spectra for a $L \approx 1$ mm long cleaved edge emitter for various pump intensities, I_P. A conversion between the pump and quantum well excitation intensity, I_{QW}, is also shown to account for various losses due to pumping the laser bars off resonance with the ArF laser. Specifically, the quantum well excitation intensity is estimated by accounting for reflection from the topside air–AlGaN surface, attenuation in the cap layer with absorption coefficient 10^5/cm, and relaxation of the generated hot electron–hole pairs to the energy band extrema, which results in emitted to absorbed photon energy ratio of 2/3. The combined effects result in a pump intensity attenuation of ~70% at the quantum well. From Fig. 3(b), as the excitation intensity is increased, the spectral FWHM decreases from ≈15 nm at I_{QW} = 195 kW/cm^2 to ≈5 nm at I_{QW} = 280 kW/cm^2 due to the onset of amplified spontaneous emission. From the output vs input power plot in Fig. 3(c), the threshold of lasing occurs at this quantum well intensity of $I_{QW} \approx$ 280 kW/cm^2. At I_{QW} = 310 kW/cm^2, this is accompanied with a broad gain spectrum with peak gain at $\lambda_0 \approx$ 284 nm and multi-mode emission is realized, as shown in Fig. 3(d). The resolution of the spectrometer is limited to ≈ 0.01 nm. However, for a laser bar of longitudinal length L and effective refractive index n_{eff}, emitting at wavelength λ_0, the modal spacing is approximately equal to $\Delta\lambda \approx \lambda_0^2/(2Ln_{eff})$.[35] For $L \approx 1$ mm and $n_{eff} \approx 3$, $\Delta\lambda \approx 0.013$ nm.[36] Since $\Delta\lambda$ is close to the spectrometer resolution, and some of the modes are suppressed, some but not all modes are resolved. The FWHM of the resolved modes is ≈0.1 nm. Similar ASE spectra are observed for the etched facet emitters, but at a higher pump intensity I_P on the order of MW/cm^2 due to a shorter cavity length of the etched facet emitters on the order of a few hundred μm. That is, the optical mirror loss scales as the inverse of the cavity length, leading to the increase in ASE threshold intensity for laser bars with a shorter cavity length.[35]

Currently, the threshold pump intensity for lasing reported here is fairly high compared to the lowest reported by MOCVD on bulk AlN,[37] while comparable to the lowest threshold intensities for stimulated emission reported by MBE on *c*-plane sapphire.[38] Yet no evidence of resonant cavity modes are presented in the MBE grown structures on foreign substrates and exhibit linewidths on the order of a few nm. Owing to the significant reduction of threshold intensity of optically pumped AlGaN laser structures is the optimization of growth conditions for the reduction of optical loss and heterostructure design for the improvement of optical gain. For the reported heterostructures here, certain straightforward experimental and design optimizations can be made to reduce the threshold pump intensity. A first example is the use of an optical pump source that is transparent for the laser cladding layers and on resonance with the active region. This enables the use of symmetric waveguides with a high confinement factor and limits device heating, which has the effect of reducing optical gain.[39,40] As another example, cavity designs other than the Fabry–Pérot resonator discussed here can be employed. These include the use of distributed Bragg reflectors based on UV-transparent oxides grown by atomic layer deposition[41] or a distributed feedback laser design enabled by electron beam lithography.[42] These techniques can be used to reduce the optical losses and threshold pump intensity but are mode-selective in nature.

In summary, multi-mode lasing is demonstrated at $\lambda_0 \approx$ 284 nm from optically excited, AlGaN double heterostructure ridge-based

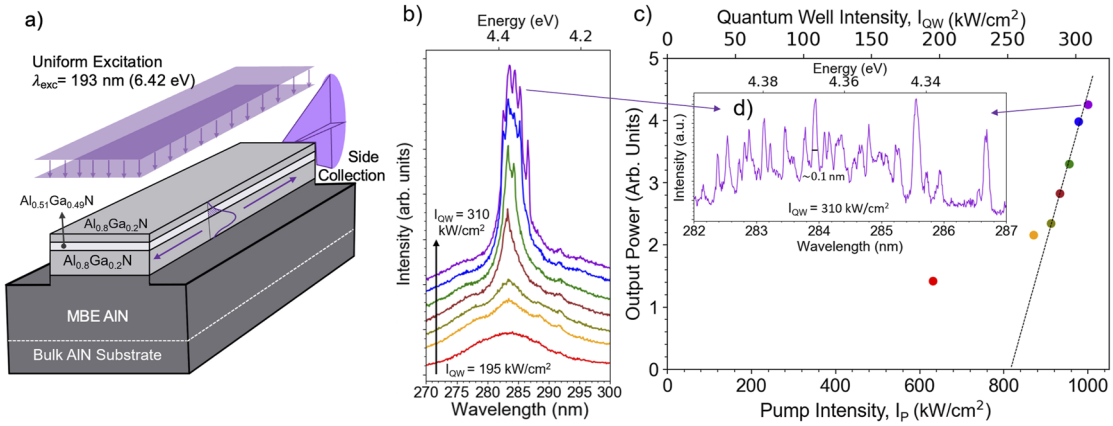

FIG. 3. (a) Schematic of an optically pumped double heterostructure AlGaN laser bar. (b) Low resolution emission spectra at different excitation intensities for a cleaved facet emitter. (c) Output power vs input power, showing lasing threshold at $I_{QW} \approx$ 280 kW/cm^2. (d) High resolution multi-mode lasing spectrum at $I_{QW} \approx$ 310 kW/cm^2.

Fabry–Pérot laser structures grown by plasma-assisted MBE on single-crystal AlN substrates. Vertical facets and ridge sidewalls were created by a combined isotropic dry and wet etch. Besides a low optical cavity loss, both electronic design optimization to maximize optical gain, as well as waveguide design and growth optimization to keep the intrinsic optical losses low, are important to achieve the more useful electrically injected, deep-ultraviolet AlGaN based laser diodes with practically large on-time or continuous wave mode capabilities. While MOCVD grown AlGaN laser diodes have achieved low optical losses, optical gain can be significantly improved to reduce the threshold current density. An example is the improvement of injection efficiency, which is currently low for MOCVD grown UV-C laser diodes.[43] Due to the absence of memory- and chemical activation-effects for Mg doping in MBE grown thin films, inverted diode structures are possible, which have been shown to improve injection efficiency in metal–polar AlInGaN n-p-i-n LEDs.[26,44] Along with the optical quality of AlGaN thin films enabled by molecular beam homoepitaxy as demonstrated for the first time here, its unique chemical and heterostructural design capabilities can be useful toward further improvement of deep-UV AlGaN laser diode technology.

The authors thank Professor Farhan Rana, Dr. Shyam Bharadwaj, and Dr. Jimy Encomendero at Cornell University for helpful discussions. This work was partially supported by the Cornell Center for Materials Research with funding from the NSF MRSEC program (Grant No. DMR-1719875). Further support was granted by ULTRA, an Energy Frontier Research Center funded by the U.S. Department of Energy (DOE), Office of Science, Basic Energy Sciences (BES), under Award No. DE-SC0021230. The authors also acknowledge the Cornell NanoScale Facility for device fabrication, supported by the National Science Foundation under Grant Nos. NNCI-2025233, RAISE-TAQS 1839196, and MRI 1631282.

AUTHOR DECLARATIONS

Conflict of Interest

The authors have no conflicts of interest to disclose.

DATA AVAILABILITY

The data that support the findings of this study are available from the corresponding author upon reasonable request.

REFERENCES

[1] D. Welch, M. Buonanno, V. Grilj, I. Shuryak, C. Crickmore, A. W. Bigelow, G. Randers-Pehrson, G. W. Johnson, and D. J. Brenner, Sci. Rep. **8**, 2752 (2018).
[2] Y. Cheng, H. Chen, L. A. Sánchez Basurto, V. V. Protasenko, S. Bharadwaj, M. Islam, and C. I. Moraru, Sci. Rep. **10**, 3411 (2020).
[3] V. Mezzanotte, M. Antonelli, S. Citterio, and C. Nurizzo, Water Environ. Res. **79**, 2373 (2007).
[4] F. Mehnke, M. Guttmann, J. Enslin, C. Kuhn, C. Reich, J. Jordan, S. Kapanke, A. Knauer, M. Lapeyrade, U. Zeimer, H. Krüger, M. Rabe, S. Einfeldt, T. Wernicke, H. Ewald, M. Weyers, and M. Kneissl, IEEE J. Sel. Top. Quantum Electron. **23**, 2000108 (2017).
[5] H. R. Allcock, M. V. B. Phelps, E. W. Barrett, M. V. Pishko, and W.-G. Koh, Chem. Mater. **18**, 609 (2006).
[6] A. Ozawa, J. Davila-Rodriguez, J. R. Bounds, H. A. Schuessler, T. W. Hänsch, and T. Udem, Nat. Commun. **8**, 44 (2017).
[7] M. A. Taylor and W. P. Bowen, Phys. Rep. **615**, 1 (2016).
[8] J. H. Park, D. Y. Kim, E. F. Schubert, J. Cho, and J. K. Kim, ACS Energy Lett. **3**, 655 (2018).
[9] H. Amano *et al.*, J. Phys. D: Appl. Phys. **53**, 503001 (2020).
[10] Z. Zhang, M. Kushimoto, T. Sakai, N. Sugiyama, L. J. Schowalter, C. Sasaoka, and H. Amano, Appl. Phys. Express **12**, 124003 (2019).
[11] K. Sato, S. Yasue, K. Yamada, S. Tanaka, T. Omori, S. Ishizuka, S. Teramura, Y. Ogino, S. Iwayama, H. Miyake, M. Iwaya, T. Takeuchi, S. Kamiyama, and I. Akasaki, Appl. Phys. Express **13**, 031004 (2020).
[12] M. Kushimoto, Z. Zhang, N. Sugiyama, Y. Honda, L. J. Schowalter, C. Sasaoka, and H. Amano, Appl. Phys. Express **14**, 051003 (2021).
[13] S. Tanaka, Y. Ogino, K. Yamada, R. Ogura, S. Teramura, M. Shimokawa, S. Ishizuka, S. Iwayama, K. Sato, H. Miyake, M. Iwaya, T. Takeuchi, and S. Kamiyama, Appl. Phys. Express **14**, 094009 (2021).
[14] A. Abare, M. Bergmann, D. Emerson, K. Haberern, T. Kuhr, and C. Hussell, in *Conference on Lasers and Electro-Optics (CLEO)* (IEEE, 2004), Vol. 2, p. 1.
[15] J. Xie, S. Mita, Z. Bryan, W. Guo, L. Hussey, B. Moody, R. Schlesser, R. Kirste, M. Gerhold, R. Collazo, and Z. Sitar, Appl. Phys. Lett. **102**, 171102 (2013).
[16] M. Martens, F. Mehnke, C. Kuhn, C. Reich, V. Kueller, A. Knauer, C. Netzel, C. Hartmann, J. Wollweber, J. Rass, T. Wernicke, M. Bickermann, M. Weyers, and M. Kneissl, IEEE Photonics Technol. Lett. **26**, 342 (2014).
[17] V. N. Jmerik, E. V. Lutsenko, and S. V. Ivanov, Phys. Status Solidi A **210**, 439 (2013).
[18] M. V. Rzheutski, E. V. Lutsenko, A. G. Vainilovich, I. E. Svitsiankou, A. V. Nahorny, G. P. Yablonskii, V. Z. Zubialevich, S. I. Petrov, A. N. Alexeev, D. V. Nechaev, and V. N. Jmerik, Phys. Status Solidi A **217**, 1900927 (2020).
[19] X. Yin and S. Zhao, Phys. Status Solidi B **257**, 2000287 (2020).
[20] H. Sun, J. Yin, E. F. Pecora, L. D. Negro, R. Paiella, and T. D. Moustakas, IEEE Photonics J. **9**, 2201109 (2017).
[21] H. Hasegawa, Y. Kamimura, K. Edagawa, and I. Yonenaga, J. Appl. Phys. **102**, 026103 (2007).
[22] D. Jena, A. C. Gossard, and U. K. Mishra, Appl. Phys. Lett. **76**, 1707 (2000).
[23] Y. Cho, C. S. Chang, K. Lee, M. Gong, K. Nomoto, M. Toita, L. J. Schowalter, D. A. Muller, D. Jena, and H. G. Xing, Appl. Phys. Lett. **116**, 172106 (2020).
[24] K. Lee, R. Page, V. Protasenko, L. J. Schowalter, M. Toita, H. G. Xing, and D. Jena, Appl. Phys. Lett. **118**, 092101 (2021).
[25] S. M. Islam, K. Lee, J. Verma, V. Protasenko, S. Rouvimov, S. Bharadwaj, H. Xing, and D. Jena, Appl. Phys. Lett. **110**, 041108 (2017).
[26] S. Bharadwaj, J. Miller, K. Lee, J. Lederman, M. Siekacz, H. Xing, D. Jena, C. Skierbiszewski, and H. Turski, Opt. Express **28**, 4489 (2020).
[27] K. Lee, S. Bharadwaj, Y.-T. Shao, L. van Deurzen, V. Protasenko, D. A. Muller, H. G. Xing, and D. Jena, Appl. Phys. Lett. **117**, 061104 (2020).
[28] R. Chaudhuri, Z. Chen, D. A. Muller, H. G. Xing, and D. Jena, J. Appl. Phys. **130**, 025703 (2021).
[29] B. Witzigmann, F. Römer, M. Martens, C. Kuhn, T. Wernicke, and M. Kneissl, AIP Adv. **10**, 095307 (2020).
[30] J. Zhang, H. Zhao, and N. Tansu, Appl. Phys. Lett. **97**, 111105 (2010).
[31] See https://www.str-soft.com/devices/silense/ for SiLENSe, STR Group.
[32] K. Iga, K. Wakao, and T. Kunikane, Appl. Opt. **20**, 2367 (1981).
[33] D. A. Stocker, E. F. Schubert, W. Grieshaber, K. S. Boutros, and J. M. Redwing, Appl. Phys. Lett. **73**, 1925 (1998).
[34] S. Yasue, K. Sato, Y. Kawase, J. Ikeda, Y. Sakuragi, S. Iwayama, M. Iwaya, S. Kamiyama, T. Takeuchi, and I. Akasaki, Jpn. J. Appl. Phys. **58**, SCCC30 (2019).
[35] S. M. Sze and K. K. Ng, *Physics of Semiconductor Devices*, 3rd ed. (Wiley, 2008), ISBN: 978-0-470-06832-8.
[36] Q. Guo, R. Kirste, P. Reddy, W. Mecouch, Y. Guan, S. Mita, S. Washiyama, J. Tweedie, Z. Sitar, and R. Collazo, Jpn. J. Appl. Phys. **59**, 091001 (2020).
[37] R. Kirste, Q. Guo, J. H. Dycus, A. Franke, S. Mita, B. Sarkar, P. Reddy, J. M. LeBeau, R. Collazo, and Z. Sitar, Appl. Phys. Express **11**, 082101 (2018).
[38] V. N. Jmerik, D. V. Nechaev, S. Rouvimov, V. V. Ratnikov, P. S. Kop'ev, M. V. Rzheutski, E. V. Lutsenko, G. P. Yablonskii, M. Aljohenii, A. Aljerwii, A. Alyamani, and S. V. Ivanov, J. Mater. Res. **30**, 2871 (2015).

[39]B. Witzigmann, V. Laino, M. Luisier, U. T. Schwarz, H. Fischer, G. Feicht, W. Wegscheider, C. Rumbolz, A. Lell, and V. Harle, IEEE Photonics Technol. Lett. **18**, 1600 (2006).
[40]L. D. Zhu, B. Z. Zheng, and G. A. B. Feak, IEEE J. Quantum Electron. **25**, 2007 (1989).
[41]T. Sakai, M. Kushimoto, Z. Zhang, N. Sugiyama, L. J. Schowalter, Y. Honda, C. Sasaoka, and H. Amano, Appl. Phys. Lett. **116**, 122101 (2020).
[42]G. Muziol, M. Hajdel, H. Turski, K. Nomoto, M. Siekacz, K. Nowakowski-Szkudlarek, M. Żak, D. Jena, H. G. Xing, P. Perlin, and C. Skierbiszewski, Opt. Express **28**, 35321 (2020).
[43]Z. Zhang, M. Kushimoto, T. Sakai, N. Sugiyama, L. J. Schowalter, C. Sasaoka, and H. Amano, Jpn. J. Appl. Phys. **59**, 094001 (2020).
[44]L. van Deurzen, S. Bharadwaj, K. Lee, V. Protasenko, H. Turski, H. G. Xing, and D. Jena, Proc. SPIE **11706**, 117060F (2021).